JOURNAL OF OPTOELECTRONICS AND ADVANCED MATERIALS Vol. 9, No. 8, August 2007, p. 2644 - 2647

Percolation phenomena in Si – SiO_2 nanocomposite films

I. STAVARACHE, M. L. CIUREA*
National Institute of Materials Physics, 077125 Bucharest - Măgurele, P.O. Box MG-7, Romania

Current – voltage characteristics of samples containing silicon nanodots embedded in an amorphous silicon dioxide matrix were investigated. A percolation mechanism was evidenced by the dependence on the concentration of the initial differential conductance and by the appearance of several thresholds in the *I – V* characteristics.

(Received May 16, 2007; after revision June 22, 2007; accepted June 27, 2007)

Keywords: Silicon nanocrystals, Electrical properties, Percolation

1. Introduction

The interest for both fundamental aspects and practical applications of the nanomaterials and nanostructures is continuously increasing. The fundamental aspects are related mainly to the quantum confinement (QC) [1 – 5] and the surface/interface effects [6 – 8]. The nanocrystalline silicon (nc-Si) is particularly important for the applications in micro- and nanoelectronics, optoelectronics, biomedical and sensor technology, due to its compatibility with the classic silicon technology.

The electrical transport in nc-Si-based materials and structures was thoroughly investigated and several mechanisms were discussed for different dimensionalities. In Si/SiO_2 superlattices, resonance tunneling between heavy and light holes QC levels was considered to explain the differential conductivity and photoconductivity peak at a given applied bias (ensuring the resonance condition) [9]. Monte Carlo simulations within the Wentzel-Kramers-Brillouin approximation were also used to describe the Si/SiO_2 superlattices [10], while Poole-Frenkel tunneling was suggested for the Si/CaF_2 multilayered structures [11]. Besides, Poole-Frenkel tunneling was proposed for the interpretation of the transport in nanocrystalline porous silicon (nc-PS) [12]. Other mechanisms taken into account for nc-PS were the hopping [13] and the fractal percolation [14]. The Schottky tunneling and the thermionic contributions were compared in ultra-small Si-based Schottky diodes, proving that the former is dominant for sizes under 100 nm [15]. On the other hand, a nanocrystalline floating gate MOS transistor was transformed into a LED through the carrier injection from the substrate, described as a Fowler-Nordheim tunneling [16]. In the case of nanocomposite films made from silicon nanodots (nc-Si) embedded in an amorphous silicon dioxide (a-SiO_2) matrix (hereafter quoted Si – SiO_2), the carrier motion inside the nanodots was proved to be ballistic [17], while the transport between the nanodots is dominated by the high field assisted tunneling (HFAT) [18]. The Coulomb blockade (CB) energy in nanodots with diameters between 4 and 6 nm is 38 – 58 meV [18], while the transversal acoustic and optic phonon energies are 19 and 56 meV respectively [5], and the room temperature (RT) thermal energy is 26 meV. Therefore, all these effects are significant only at low field ($eU << k_BT$). However, it is obvious that the tunneling becomes significant only over a percolation threshold.

In this paper, the percolation processes in Si – SiO_2 nanocomposite films are investigated. Section 2 deals with the preparation and microstructure of the films. In Section 3, the *I – V* characteristics are investigated in order to evidence the percolation phenomena and the results are discussed. The last Section presents the concluding remarks.

2. Preparation and microstructure

Our Si – SiO_2 films were prepared by co-sputtering Si and SiO_2 from two targets located 5 cm below the quartz slide substrate [18–20]. After the sputtering, the samples were annealed at 1100 ^oC in N_2 atmosphere, in order to nucleate Si nanocrystallites. Under these conditions, the Si – SiO_2 samples obtained at a single deposition have 9 μm thickness and variable nc-Si volume concentration (from $x \approx 0$ to 100%) while the mean nanodot diameters vary slowly with x [21]. 50 parallel Al electrodes (2 mm width) were deposited in a coplanar configuration (1 mm interspace). As the nc-Si concentration varies almost linear with the position [18, 19], its mean value between two consecutive electrodes is determined with an absolute error of 0.67 %, estimated from the ratio between the distance between two consecutive electrodes and the total length of the sample.

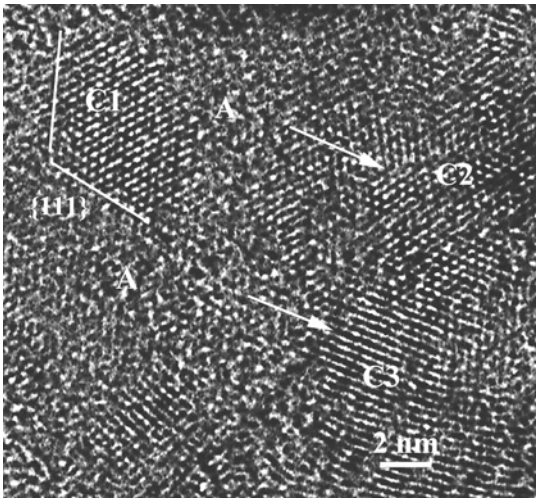

Fig. 1. HRTEM image of Si – SiO_2 nanocomposite ($x \approx 50$ %). C1 to C3 are Si nanodots and A is amorphous SiO_2. The fringes show the relative orientation of the nanodots (C2 and C3 almost parallel, C3 rotated clockwise with about 30°).

A high resolution transmission electron microscopy image of the Si – SiO_2, taken from the region with nc-Si volumic concentration of about 50 vol. %, is presented in Fig. 1. One can observe that the Si nanodots have almost equal sizes and tend to form chains separated by a-SiO_2. This suggests that the transport is dominated by a percolation network.

3. Results and discussion

The current–voltage (I–V) characteristics at room temperature (RT) were taken using Keithley 642 and Keithley 6517A electrometers, a Keithley 2000 multimeter, and an Agilent E3631A d.c. power supply, ensuring relative errors of no more than 0.01 % in both current and voltage measurements. The results are presented in Figs. 2 and 3.

From the insert in Fig. 2, one can see that the percolation threshold is $x_t \approx 34.7$ % (the mean value of the two concentrations). Indeed, at $x \approx 33.7$ %, the noise is of the same order of magnitude ($2 \cdot 10^{-13}$ A) as the current at 2 V bias, while at $x \approx 35.7$ %, the current is one order of magnitude greater. The 2 V bias was chosen as test value because of the CB. A previous investigation of the $I - V$ characteristics, made at $x \approx 66$ % [18], proved that the CB threshold at RT is 1.75 V. As the CB threshold is roughly proportional with the cubic root of the number of nanodots, it means that its value at $x \approx 34.7$ % is about 1.4 V. Then the limitation of the bias under 2 V in search of the percolation threshold is covering.

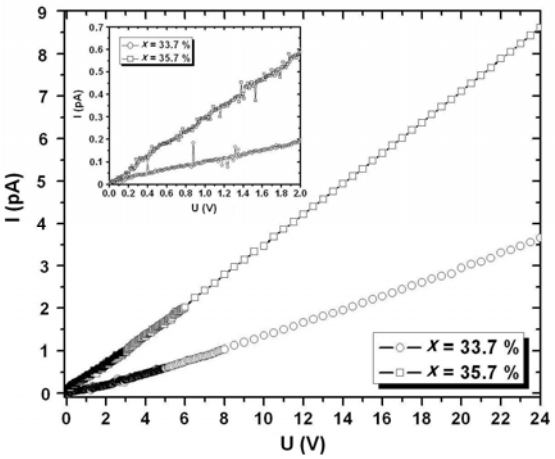

Fig. 2. I – V characteristics around the percolation threshold ($x_t \approx 34.7$ %).

On the other hand, the measurements performed up to 25 V at the same concentrations present an Ohmic behavior. This suggests that, at concentrations close to the percolation threshold, the transport is dominated by the conduction of the impurity ions from the a-SiO_2 as well as of the electrons and holes from the band tails.

Significant measurements made at intermediate nc-Si concentrations are presented in Fig. 3. One can see that the current is two orders of magnitude greater. At the same time, the characteristics are dominated by the HFAT mechanism, described by the relation [18]:

$$I = I_0 \mathrm{sign}(U)\left[\left(1-|U|/U_0\right)\times\exp\left(-\alpha\sqrt{1-|U|/U_0}\right)-\exp(-\alpha)\right], \quad (1)$$

where $U_0 = N\varphi/e$, $\alpha = \delta\chi\varphi^{1/2}$ and $\chi = (8m^*/\hbar^2)^{1/2}$ (m^* being the effective carrier mass and N the mean number of tunneled barriers of height φ and width δ). Several small percolation thresholds appear at 16, 18, for $x \approx 39.8$ %, and 17.2, at 19.1, 20.6, and 22.1 V for $x \approx 43.9$ %. These thresholds are related to the possibility of tunneling larger barriers with the increase of the bias. It is remarkable that the higher voltage thresholds are practically the same for the two concentrations.

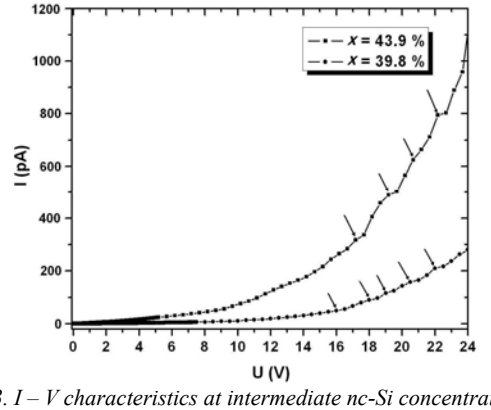

Fig. 3. I – V characteristics at intermediate nc-Si concentrations. The percolation thresholds are marked with arrows.

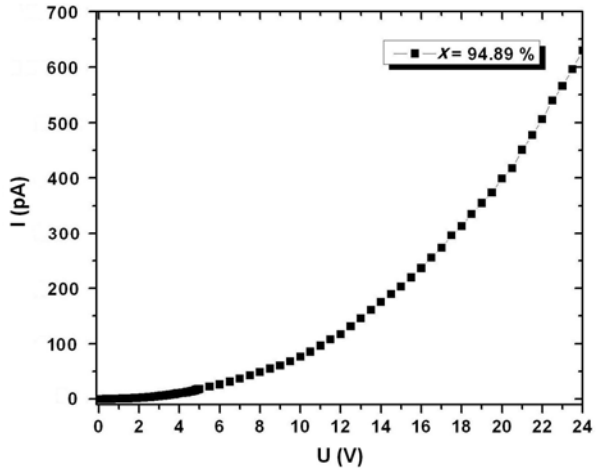

Fig. 4. I – V characteristic at high nc-Si concentration.

Fig. 4 presents a characteristic obtained at high nc-Si concentration. One can observe the disappearance of the percolation thresholds, as now several paths of similar resistance are available. The random distribution of the Si nanodots makes N to fluctuate as function of x, so that the fact that the current is smaller that at lower concentration is due to such fluctuations.

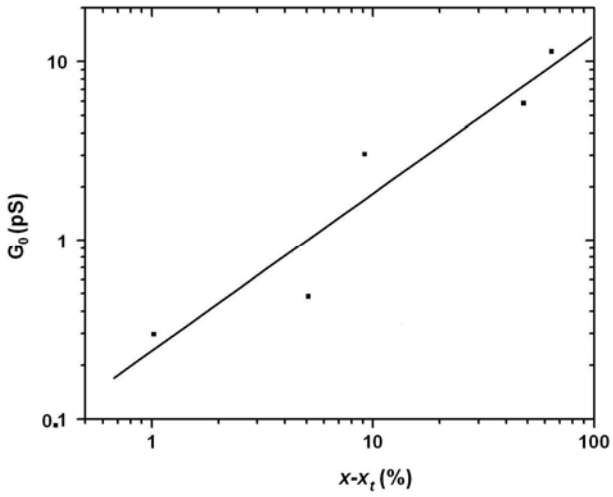

Fig. 5. Conductance dependence on the nc-Si concentration.

In order to check the percolation mechanism, the initial differential conductance G_0:

$$G_0 = (dI/dV)_{V=0} \tag{2}$$

was evaluated (with relative errors of 1 %) as function of the nc-Si concentration. The results are represented in Fig. 5. The points corresponding to high concentrations are not represented, because of the disappearance of the percolation mechanism. One can see that:

$$G \propto (x - x_t)^{\gamma}, \tag{3}$$

i.e. a typical percolation characteristic [22, 23], with the critical exponent $\gamma = 0.8824 \pm 0.0029$. It is remarkable that this dependence extends from the Ohmic to the HFAT behavior, where the initial differential conductance is:

$$G_0 = \frac{I_0}{U_0}\left(\frac{\alpha}{2} - 1\right)\exp(-\alpha). \tag{4}$$

This proves that the percolative behavior does not depend on the local transport mechanism, but only on the nanodots distribution. It is also interesting to note the agreement with the critical exponent previously found on PS ($\gamma = 0.88$, see [24]).

4. Conclusions

Current–voltage characteristics taken on $Si–SiO_2$ nanocomposite films at different nc-Si concentrations were analyzed. A percolative behavior was evidenced by (i) the identification of a critical concentration ($x_t \approx 34.7$ %) that forms the percolation threshold, (ii) the identification of several voltage thresholds, (iii) the power dependence of the conductance on the concentration (critical exponent $\gamma \approx 0.88$), and (iv) the fact that this dependence extends from Ohmic to HFAT transport mechanisms.

Acknowledgements

This work was supported from CEEX 0611-13/2006 Research Contract.

References

[1] K. Clemenger, Phys. Rev. B **44**, 12991 (1991).
[2] W. P. Yuen, Phys. Rev. B **48**, 17316 (1993).
[3] M. L. Ciurea, I. Baltog, M. Lazar, V. Iancu, S. Lazanu, E. Pentia, Thin Solid Films **325**, 271 (1998).
[4] E. Lampin, C. Delerue, M. Lannoo, G. Allan, Phys. Rev. B **58**, 12004 (1998).
[5] J. Heitmann, F. Müller, L. X. Yi, M. Zacharias, D. Kovalev, F. Eichhorn, Phys. Rev. B **69**, 195309 (2004).
[6] D. A. Faux, J. R. Downes, E. P. O'Reilly, J. Appl. Phys. 82, 3754 (1997).
[7] A. Benfilda, Proc. 1st Int. Workshop Semicond. Nanocryst. SEMINANO 2005, Budapest 2005, **1**, 123.
[8] C. Baratto, G. Faglia, G. Sberveglieri, Z. Gaburro, L. Pancheri, C. Oton, and L. Pavesi, Sensors **2**, 121 (2002).
[9] B. V. Kamenev, G. F. Grom, D. J. Lockwood, J. P. McCafrey, B. Laikhtman, L. Tsybeskov, Phys. Rev. B **69**, 235306 (2004).

[10] M. Rosini, C. Jacoboni, S. Ossicini, Phys. Rev. B **66**, 155332 (2002).
[11] V. Ioannou-Sougleridis, T. Ouisse, A. G. Nassiopoulou, F. Bassani, F. Arnaud d'Avitaya, J. Appl. Phys. **89**, 610 (2001).
[12] M. Ben-Chorin, F. Möller, F. Koch, Phys. Rev. B **49**, 2981 (1994).
[13] N. Koshida, H. Koyama, Mater. Res. Soc. Symp. Proc. **283,** 337 (1993).
[14] M. Ben-Chorin, F. Möller, F. Koch, Phys. Rev. B **51,** 2199 (1995).
[15] G. D. J. Smit, S. Rogge, T. M. Klapwijk, Appl. Phys. Lett. **81**, 3852 (2002).
[16] R. J. Walters, G. I. Bourianoff, H. A. Atwater, Nature Materials **4**, 143 (2005).
[17] T. V. Torchynska, J. Appl. Phys. **92**, 4019 (2002).
[18] M. L. Ciurea, V. S. Teodorescu, V. Iancu, I. Balberg, Chem. Phys. Lett. **423**, 225 (2006).
[19] M. Dovrat, Y. Oppenheim, J. Jedrzejewski, I. Balberg, A. Sa'ar, Phys. Rev. B **69**, 155311 (2004).
[20] V. Iancu, M. Draghici, L. Jdira, M. L. Ciurea, J. Optoelectron. Adv. Mater. **6**, 53 (2004).
[21] V. S. Teodorescu, M. L. Ciurea, V. Iancu, M. G. Blanchin, Proc. IEEE CN 04TH8748, Int. Semicond. Conf. CAS 2004, Sinaia, 3 – 6 October 2004, **1**, 59 (2004).
[22] S. H. Munson-McGee, Phys. Rev. B, **43**, 3331 (1991).
[23] Yu Jin Chang, Byung Hyun Kang, Gyu Tae Kim, Sung Joon Park, Jeong Sook Ha, Appl. Phys. Lett. **84**, 5392 (2004).
[24] E. Axelrod, A. Givant, J. Shappir, Y. Feldman, A. Sa'ar, J. Non-Crystal. Solids, **305**, 235 (2002).

* Corresponding author: ciurea@.infim.ro